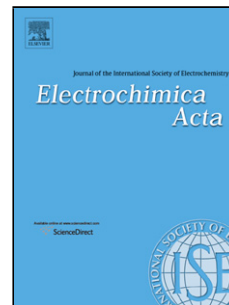


## Accepted Manuscript

Title: Investigation of the *N*-butyl-*N*-methyl pyrrolidinium trifluoromethanesulfonyl-*N*-cyanoamide (PYR<sub>14</sub>TFSAM) ionic liquid as electrolyte for Li-ion battery

Authors: Jan-Philipp Hoffknecht, Mathias Drews, Xin He, Elie Paillard



PII: S0013-4686(17)31647-X  
DOI: <http://dx.doi.org/doi:10.1016/j.electacta.2017.08.020>  
Reference: EA 30024

To appear in: *Electrochimica Acta*

Received date: 9-5-2017  
Revised date: 7-7-2017  
Accepted date: 5-8-2017

Please cite this article as: Jan-Philipp Hoffknecht, Mathias Drews, Xin He, Elie Paillard, Investigation of the *N*-butyl-*N*-methyl pyrrolidinium trifluoromethanesulfonyl-*N*-cyanoamide (PYR<sub>14</sub>TFSAM) ionic liquid as electrolyte for Li-ion battery, *Electrochimica Acta* <http://dx.doi.org/10.1016/j.electacta.2017.08.020>

This is a PDF file of an unedited manuscript that has been accepted for publication. As a service to our customers we are providing this early version of the manuscript. The manuscript will undergo copyediting, typesetting, and review of the resulting proof before it is published in its final form. Please note that during the production process errors may be discovered which could affect the content, and all legal disclaimers that apply to the journal pertain.

**Investigation of the *N*-butyl-*N*-methyl pyrrolidinium  
trifluoromethanesulfonyl-*N*-cyanoamide (PYR<sub>14</sub>TFSAM) ionic liquid as  
electrolyte for Li-ion battery**

Jan-Philipp Hoffknecht<sup>a</sup>, Mathias Drews<sup>a</sup>, Xin He<sup>a</sup>, Elie Paillard<sup>a\*</sup>

<sup>a</sup>*Helmholtz Institute Münster – Forschungszentrum Jülich GmbH (IEK 12), Corrensstrasse 46, 48149*

*Münster, D-48149 Münster, Germany*

*e.paillard@fz-juelich.de*

\* Corresponding author: [e.paillard@fz-juelich.de](mailto:e.paillard@fz-juelich.de)

**Abstract**

A new asymmetrical anion, trifluoromethanesulfonyl-*N*-cyanoamide (TFSAM<sup>-</sup>), was paired with *N*-butyl-*N*-methyl pyrrolidinium (PYR<sub>14</sub><sup>+</sup>) to prepare PYR<sub>14</sub>TFSAM. It has been investigated for Li-ion battery application and compared to its PYR<sub>14</sub><sup>+</sup> analogs paired with either the dicyanamide anion (DCA<sup>-</sup>) or other anions (*i.e.* bis(trifluoromethanesulfonyl) imide (TFSI<sup>-</sup>), bis(fluorosulfonyl)imide (FSI<sup>-</sup>), trifluoromethanesulfonyl-fluorosulfonyl imide (FTFSI<sup>-</sup>)). The conductivity of PYR<sub>14</sub>TFSAM is not only higher than that of PYR<sub>14</sub>TFSI, but also higher than that of PYR<sub>14</sub>FTFSI with 3.8 mS cm<sup>-1</sup> at 20°C and 12.6 mS cm<sup>-1</sup> at 60°C. In addition, the ionic liquid does not crystallize and exhibits a viscosity similar to that of PYR<sub>14</sub>FSI (and even lower above 30°C, which also results in a higher conductivity at high temperature). Compared to PYR<sub>14</sub>DCA, PYR<sub>14</sub>TFSAM has a higher anodic stability, more compatible with state-of-the-art cathodes such as NCM, even though the PYR<sub>14</sub>DCA electrolyte also allowed surprisingly good cycling results of NCM cathode considering its low anodic stability. PYR<sub>14</sub>TFSAM also allows Li<sup>+</sup> (de-)/insertion into graphite, using vinylene carbonate as additive. When used in conventional Li-ion electrolyte solvents, it leads to moderate conductivity (as compared with LiFSI or

LiTFSI), although much higher than LiDCA. Additionally, it is shown that, even in EC/DMC-based electrolyte, LiTFSAM does not induce Al corrosion at 4.2V.

**Keywords:** Pyrrolidinium; ionic liquid; electrolyte; Li-ion; Li metal; trifluoromethanesulfonyl-*N*-cyanoamide; TFSAM; asymmetrical anion; lithium dicyanamide; LiDCA; LiTFSAM; ethylene carbonate; dimethyl carbonate; vinylene carbonate; NCM; NMC; graphite.

## 1. Introduction

Li-ion batteries have become part of modern life and are now present in most portable electronic devices. However, as their uses extend to larger applications such as electric vehicles (EVs) and stationary storage for grid levelling, the question of their safety and sustainability must be addressed. Indeed, state-of-the-art Li-ion electrolytes are mixtures of cyclic and linear alkyl carbonates and contains  $\text{LiPF}_6$  as lithium salt. While linear alkyl carbonates are highly volatile, flammable and have very low flash points[1],  $\text{LiPF}_6$  decomposes at *ca.* 60°C in presence of water traces[2,3] or electrolyte components[4]. Moreover, it is readily hydrolyzed in ambient atmosphere to hydrofluoric acid and thus cannot be recycled. Thus, alternatives have been sought for improving the safety of Li-ion batteries and flame retardants[1,5,6], as well as higher flash point solvents such as sulfones[7] and dinitriles[1,8] have been proposed. Lithium salts with higher stabilities toward hydrolysis and temperature such as lithium bis(trifluoromethanesulfonyl)imide (LiTFSI)[9] or lithium bis(fluorosulfonyl)imide (LiFSI)[10], shown in figure 1, have also been proposed. However, the choice of lithium salt is, *in fine*, a compromise between many practical considerations such as price, solubility, conductivity, anodic stability in the solvent mixture used, as well as the possibility to form of a good solid electrolyte interphase (SEI) [11,12] at the anode (*i.e.* a passivation layer needed for the operation of graphite electrodes). Moreover, the passivation of aluminum current collectors is needed, for which LiTFSI is known to be detrimental, while LiFSI is controversial[10,13].

One of the most promising approach for higher temperature applications of Li-ion batteries, such as EVs and stationary storage (as the cooling of large batteries is more challenging than that of low power batteries), is the use of ionic liquid (ILs)-based electrolytes. They have been proposed both for Li-metal batteries, either as liquid[14,15] or as plasticizers for PEO-based electrolytes[16,17] and for Li-ion batteries[18,19]. While their properties (protic, aprotic, hydrophobic hydrophilic, flammable or not) depends on their constituents, those based one the TFSI<sup>-</sup> anion and quaternary ammonium cations are hydrophobic, possess high oxidative and thermal stability, negligible vapor pressure and flammability and allow decent Li metal anode operation[14,20]. However, TFSI<sup>-</sup> molecular weight induces high viscosities at room temperature, which limits the conductivities of the resulting ionic liquids. ILs incorporating smaller anions such as dicyanamide (DCA<sup>-</sup>)[21–24] or bis(fluorosulfonyl)imide (FSI<sup>-</sup>) [18,25], shown on figure 1, allow obtaining lower viscosities and higher conductivities. In fact, the DCA<sup>-</sup> anion leads to ILs with among the lowest viscosities and highest conductivities. However, replacing the -SO<sub>2</sub>-CF<sub>3</sub> groups by -CN electron withdrawing substituents (as compared to the formula of TFSI<sup>-</sup>, see figure 1), if it allows decreasing the size of the anion, is still not enough for ensuring high oxidative stability for a use in state-of-the-art Li-ion batteries (i.e. operating up to 4.2-4.3V). Moreover, the stability of the DCA<sup>-</sup> anion in reduction (and especially versus graphite anodes) is not well established, although PYR<sub>14</sub>DCA has been proposed for Li metal batteries[22]. Nevertheless, even the low potential LiFePO<sub>4</sub> cathode does not lead to high efficiencies in PYR<sub>14</sub>DCA and its use seems, so far, limited to electrochemical double layer capacitors operating at 2.6 V[24]. It could however be possible that Li-ion batteries can operate upon a wider electrochemical window in this electrolyte, thanks to passivation layers (SEI) formations that might form at the anode (and possibly cathode).

## FIGURE 1

Several factors influence the performance of ILs. First of all, their liquid range depends on their ability to crystallize which can lead to either low melting point or amorphous ILs. It depends on the strength of the interactions between anion and cation, their symmetry, as well as their conformational flexibility (i.e. having different conformers of low energy)[26,27] as these impact the formation of crystalline phases which require a regular space arrangement of their constituent with well-defined orientation and

conformation. If the use of asymmetrical cations is relatively common[28], ILs incorporating low symmetry anions have also been proposed [29–31] for decreasing further the asymmetry within ILs and suppressing their crystallization. This can also be achieved by mixing different ionic liquids [32], especially with those which do not crystallize[33]. In particular, the fluorosulfonyl-trifluoromethanesulfonyl imide anion (FTFSI<sup>-</sup>), shown in figure 1, is an asymmetrical hybrid between the FSI<sup>-</sup> and TFSI<sup>-</sup> anion and displays a higher thermal stability than FSI<sup>-</sup>. In addition, its ILs have viscosities and conductivities closer to those of the FSI<sup>-</sup> analogs with the main advantage of being amorphous, thus liquid and conductive on a wide temperature window, thanks to its asymmetry[31].

In this work, we examine the physico-chemical properties of the trifluoromethanesulfonyl cyano amide (TFSAM<sup>-</sup>) anion, shown in figure 1, which is an asymmetrical hybrid between the TFSI<sup>-</sup> and the DCA<sup>-</sup> anions. This anion was first synthesized and reported by Shaplov *et al.*[34] and various ILs were prepared with this anion and showed an improved anodic stability as compared with DCA analogs, high conductivities and high thermal stabilities. Thus, we compare here the electrochemical performance of the DCA<sup>-</sup> and TFSAM<sup>-</sup> anions, in the IL form, combined with the *N*-methyl-*N*-butyl pyrrolidinium cation (PYR<sub>14</sub><sup>+</sup>) for a use in Li-ion battery and compare their properties with several PYR<sub>14</sub>-based ILs incorporating other known promising anions.

## 2. Experimental

### 2.1 Chemicals used

Acetonitrile (99.9%, Merck), Potassium (2,2,2- trifluoromethylsulfonyl)-*N*-cyanoamide (KTFSAM) (97%, PROVISCO), *N*-methyl pyrrolidine (99.5%, Aldrich), , *N*-methyl pyrrolidone (99.5% Acros), PYR<sub>14</sub>DCA (99.9%, Solvionic SA) and NaDCA (99%, Aldrich), Lithium 4,5 dicyano-2-(trifluoromethyl)imidazole (LiTDI) (Solvionic S.A.) and PYR<sub>14</sub>TDI (Solvionic S.A.) were used as received. Bromobutane (99% Aldrich), *N*-methyl pyrrolidone (99.5% Acros) were distilled before use. Dichloromethane (99.9%, Merck) was freshly purified by a PureSolv™ solvent purification system (INNOVATIVE TECHNOLOGY)

### 2.2 Purity analysis

Ionic Chromatography (IC) was used to investigate the possible contamination of salts and ILs by chloride or bromide impurities, using an 850 Professional IC (Metrohm) equipped with a ASUpp7-250x4.0 mm column. A 3.6 mM Na<sub>2</sub>CO<sub>3</sub> solution in water with 45% acetonitrile was used as an eluent. The samples were diluted (1:10 with water or ACN). Quantification was done via standard solutions (1, 2, 5 and 10 ppm of chloride and bromide) and the measurement were run at 65°C.

NMR: NMR experiments were performed on BRUKER AVANCE I (300 MHz) and BRUKER AVANCE III (400 MHz) devices. All samples were prepared under argon atmosphere in deuterated solvents. The solvent signals were used as reference. The data was analyzed with the TOPSPIN™ software (BRUKER). Characterization was done by means of chemical shift (in ppm), coupling constant (J in Hz), intensity and multiplicity (s singlet, d duplet, dd duplet in duplet, t triplet, q quartet).

### 2.3 Preparation of lithium dicyanamide (LiDCA)

Following a procedure reported in the literature [35], the reaction of sodium dicyanamide (10.0 g, 112 mmol, 1.0 eq) and lithium chloride (4.75 g, 112 mmol, 1.0 eq) in THF (120 mL) at 90 °C for 3 d yielded a colorless solid. The crude product was purified by multiple recrystallization from acetonitrile to gain the title compound (5.90 g, 80.8 mmol, 72%). IC results: 0 ppm bromide, 9.7 ppm chloride.

### 2.4 Preparation of *N*-butyl-*N*-methyl pyrrolidinium (PYR<sub>14</sub>Br)

PYR<sub>14</sub>Br was prepared according to an already published procedure [28] using freshly distilled bromobutane and *N*-methyl pyrrolidine in stoichiometric amounts in ethyl acetate. The reaction vessel was maintained at 0°C for 2 hrs, left to reach room temperature and further stirred for 24h. The white crystals were then filtrated and washed 3 times in fresh ethyl acetate. The residual solvent was evaporated and the PYR<sub>14</sub>Br compound was then dried at 80°C for 24h under vacuum.

### 2.5 Preparation of *N*-butyl-*N*-methyl-pyrrolidinium (2,2,2- trifluoromethylsulfonyl)-*N*-cyanoamide (PYR<sub>14</sub>TFSAM)

PYR<sub>14</sub>TFSAM, was prepared according to the procedure published by Shaplov *et al.*[34], modified as follows: *N*-butyl-*N*-methyl-pyrrolidinium bromide (20.0 g, 90.0 mmol, 1.0 eq) was dissolved in deionized water and cooled down to 0 °C. Potassium (2,2,2- trifluoromethylsulfonyl)-*N*-cyanoamide (21.0 g, 99.4

mmol, 1.1 eq) was added dropwise as aqueous solution. After stirring at 0 °C for 1 h, the reaction was allowed to warm up and was stirred for additional 12 h at r.t. Thereafter, the reaction mixture was extracted with CH<sub>2</sub>Cl<sub>2</sub> (3 x 50 mL). The combined organic layers were washed four times with equivolumes of deionized water, dried over Na<sub>2</sub>SO<sub>4</sub> and the solvent was removed under reduced pressure. The obtained light yellow liquid was redissolved in acetonitrile and stirred with activated carbon for 18 h. The suspension was filtrated and the solvent removed in vacuum. The product was obtained as colorless liquid (25.0 g, 79.3 mmol, 88% yield).

<sup>1</sup>H NMR (400 MHz, CD<sub>3</sub>CN) [ppm]: δ = 0.93 (3H, t, J=7.36 Hz, CH<sub>2</sub>-CH<sub>2</sub>-CH<sub>2</sub>-CH<sub>3</sub>), 1.34 (2H, q, J=7.40 Hz, CH<sub>2</sub>-CH<sub>2</sub>-CH<sub>2</sub>-CH<sub>3</sub>), 1.70 (2H, m, J=7.97 Hz, CH<sub>2</sub>-CH<sub>2</sub>-CH<sub>2</sub>-CH<sub>3</sub>), 2.13 (4H, s, CH<sub>2</sub>-ring), 2.94 (3H, s, N-CH<sub>3</sub>), 3.23 (2H, t, J=8.52 Hz, CH<sub>2</sub>-CH<sub>2</sub>-CH<sub>2</sub>-CH<sub>3</sub>), 3.40 (4H, d, J=3.20 Hz, N-CH<sub>2</sub>-ring).

<sup>13</sup>C NMR (100 MHz, CD<sub>3</sub>CN) [ppm]: δ = 13.40 (1C, s), 19.92 (1C, t, J=1.50 Hz), 21.87 (1C, s), 25.80 (1C, s), 48.67 (1C, d, J=3.87 Hz), 64.55 (1C, t, J=2.92 Hz), 64.80 (1C, d, J=2.38 Hz).

IC (0.7 mL / min, 65 °C): 2.9 ppm Br<sup>-</sup>, 6.5 ppm Cl<sup>-</sup>.

## 2.6 Electrode preparation

NCM electrodes: Using a zirconia ball-milling jar and zirconia balls, 1.6 g of LiNi<sub>0.5</sub>Co<sub>0.2</sub>Mn<sub>0.3</sub>O<sub>2</sub> (NCM) active material (NCM523, Cabot), 200 mg of carbon black (Super C65, IMERYYS) and 200 mg of PVdF binder (Solef 6020, Solvay), i.e. 4 g of a 5 wt% solution in *N*-methyl pyrrolidone (NMP) and 2 mL additional NMP were mixed using a planetary ball milling machine (Fritsch Pulverisette 7) ( $m_{\text{balls}}/m_{\text{AM}} = 10/1$ ) to prepare the slurry (30 min rotation, 600 rpm, 10 min rest, 3 repetitions) with a 80/10/10 mass ratio of active material/carbon black/binder. The slurry was coated on an aluminum foil previously washed with ethanol and dried. After drying the electrode sheets at 100 °C for 24 h, electrodes (12 mm Ø) were punched and dried in vacuum at 120 °C for 24 h. The mass active loading of the electrodes was ca. 2 mg cm<sup>-2</sup>

Graphite electrodes: In a 40 mL vial, 3.6 g of graphite active material (SMG-A4, Hitachi Chemicals), 200 mg of carbon black (Super C65, IMERYYS) and 200 mg of carboxymethyl cellulose (CMC) binder (WALOCCEL CRT 2000 PPA 12, Dow Wolff Cellulosic), i.e. 10 g of a 2 wt% solution in water, were

weighed in. The mixture was stirred on a magnetic stirrer for 1 h then dispersed using a dispersion system (Dispermat™ VL, VMA GmbH) (10000 rpm, 1 h). The slurry, with a 90/5/5 mass ratio of active material/carbon black/binder, was coated on a copper foil previously washed with ethanol. After drying the electrode sheets at 80 °C for 24 h, electrodes (12 mm Ø) were punched and dried in vacuum at 80 °C for 48 h. The active mass loading of the electrodes was ca. 2 mg cm<sup>-2</sup>

## 2.7 Electrolyte preparation

All electrolytes were prepared under argon atmosphere, using dry lithium salts and ionic liquids (dried at 60°C for respectively 24h and 72h, using a turbo molecular pump (vacuum reaching 10<sup>-7</sup> Bar)) and solvents (as received and kept in a glove box with H<sub>2</sub>O and O<sub>2</sub> levels below 1 ppm). The desired amount of salt was weighed in volumetric flask, pre-dissolved in half of the solvent, before completely filling the flask. In the case of electrolytes based on ILs, a light heating at 50 °C was applied.

## 2.8 Electrochemical testing

Cells preparation: For the electrochemical characterizations, three electrode SWAGELOK® cells were used. The cell assembly was done in a glovebox under argon atmosphere with H<sub>2</sub>O and O<sub>2</sub> content below 1 ppm. Metallic lithium foil (99.99%, Rockwood Lithium) was used as counter and reference electrodes (CE and RE). Depending on the investigation, different working electrodes were used: nickel, platinum, aluminum, NCM and graphite. The WE and CE were separated by either a FREUDENBERG FS2226 fleece, 13 mm Ø, six layers (for EC/DMC-based electrolytes) or a WHATMAN® GF/D glass, 13 mm Ø, one layer fiber (for ionic liquid based electrolytes) soaked with electrolyte (120 µL). On the RE side, a 10 mm Ø separator soaked with electrolyte (80 µL) was used. When using ionic liquid electrolytes, vacuum was applied to the cells before sealing them, to ensure good electrode wetting of electrodes and separator.

Linear voltamperometry: To test the cathodic (resp. anodic) stability, a freshly polished Ni (resp. Pt) electrode was polarized from the open-circuit potential to -0.5V (resp. 6.0V) at 0.1 mV s<sup>-1</sup>.

Cyclic Voltammetry (CV): For lithium plating/stripping, the CV scans were done using a Ni electrode as WE. Starting at open circuit potential (OCP), the potential was scanned at 0.1 mV s<sup>-1</sup> down to -0.5 V

vs.  $\text{Li}^+/\text{Li}$ , then reversed to 0 V vs. OCP.  $\text{Li}^+$  insertion into graphite electrodes was done starting at OCP, the potential was scanned at  $0.05 \text{ mV s}^{-1}$  down to 0 V vs.  $\text{Li}^+/\text{Li}$ , then reversed to 0 V vs. OCP.

Chronoamperometry: To investigate aluminum pitting corrosion, chronoamperometry was performed using aluminum current collectors as WEs. After a linear sweep voltammetry from OCP to 4.2 V vs.  $\text{Li}^+/\text{Li}$ , the potential was hold at 4.2 V for 12 h.

The conductivity of the electrolytes was measured using an impedance-based conductimeter (MCS10 Bio-logic). The conductivity cells were calibrated before use with a standard KCl solution. The cells were sealed in a glovebox. The temperature was varied with 20 min ramps every  $5^\circ\text{C}$  (followed by stabilization at each temperature, monitored by conductivity measurements), in decreasing steps. For  $\text{PYR}_{14}\text{TDI}$ , the temperature was ramped in both directions to acquire conductivity in the (metastable) liquid state below the melting point.

## 2.9 Thermal analysis

Differential scanning calorimetry (DSC) was done on a Q2000 DSC (TA instruments) calibrated with indium, under He flow, at  $10^\circ\text{C min}^{-1}$  in aluminum (TZero™) pans sealed in dry room with dew point below  $-50^\circ\text{C}$ . The glass transition temperatures ( $T_g$ ) were taken at the inflexion points of the baselines. Thermogravimetric analysis (TGA) was done on a Q5000 TGA (TA instruments) under  $\text{N}_2$  and artificial air (*i.e.* a mixture of  $\text{O}_2$  and  $\text{N}_2$ ). For TGA experiments, the samples were exposed to ambient air prior to the measurements.

## 2.10 Viscosity and density

Viscosity was measured using a rheometer (Anton Paar, MCR 301) at constant shear rate ( $1000 \text{ s}^{-1}$ ) located in a dry room with dew point below  $-50^\circ$ .

Density was measured using a Density Meter (METTLER TOLEDO DE40) located in a dry room with dew point below  $-50^\circ\text{C}$ .

## 2.11 Fitting of curves

Data analysis was done using a MATLAB R2016a version. Vogel Tammann Fulcher (VTF) fits for conductivity and viscosity data and the corresponding error values were calculated using a least square method.

### 3 Results and discussion Thermal characterizations

The thermal properties measured for of PYR<sub>14</sub>TFSAM and PYR<sub>14</sub>DCA are summarized in table 1.

The TGA traces of PYR<sub>14</sub>DCA and PYR<sub>14</sub>TFSAM under N<sub>2</sub> and artificial air are shown in figure 2a. The weight losses start at similar temperatures in air and N<sub>2</sub> in both cases. PYR<sub>14</sub>TFSAM exhibit a higher decomposition temperature, at *ca.* 283°C, while that of PYR<sub>14</sub>DCA is lower, starting at *ca.* 238°C. Both values are consistent with the reported values for PYR<sub>13</sub>TFSAM (285°C)[34] and PYR<sub>12</sub>DCA (250°C)[21]. The thermal stability is, in addition, higher than the reported values for PYR<sub>14</sub>FTFSI in N<sub>2</sub> and O<sub>2</sub> (256°C and 202°C respectively)[31]. The values are, however, lower than that of PYR<sub>14</sub>TFSI (above 300°C in N<sub>2</sub>[36]). However, even for PYR<sub>14</sub>DCA, the stability is significantly higher than the upper limit for any carbonate-based electrolytes.

## FIGURE 2

The DSC thermograms of PYR<sub>14</sub>DCA and PYR<sub>14</sub>TFSAM are shown in Figure 2c. Both compounds remain amorphous on the cooling ramp (not shown), exhibiting only their T<sub>g</sub>. On the heating ramps, they show similar glass transition temperatures. In fact, the T<sub>g</sub> of PYR<sub>14</sub>TFSAM (-97.7°C) is only slightly higher than that of PYR<sub>14</sub>DCA (-98.9°C), (*i.e.* slightly higher than reported previously[21]), but significantly lower than that of PYR<sub>14</sub>TFSI (-85°C)[32]. For the TFSAM<sup>-</sup> anion, the T<sub>g</sub> contrasts with that reported for PYR<sub>13</sub>TFSAM (-12°C), which is excessively high for ILs with high conductivity and low viscosity and might have been an artifact (or a typo), PYR<sub>13</sub><sup>+</sup>-based ionic liquids having usually lower viscosity and T<sub>g</sub> than their PYR<sub>14</sub><sup>+</sup> counterparts. Moreover, for PYR<sub>14</sub>DCA, a clear melting transition can be observed. On the heating ramp, a cold crystallization starts at *ca.* -55°C, followed by an endothermic melting peak starting slightly before -15.5 °C with an corresponding

enthalpy  $\Delta H_m = 110.0 \text{ J g}^{-1}$ . This contrasts with previous report as only a weak transition was reported around  $-55^\circ\text{C}$ [21]. It could be due to the fact that ionic liquids often present different phase behavior, depending on the thermal history, sample size or purity[37] and can remain amorphous below their melting point for extended period of time. In fact, their tendency to stay in a metastable liquid state (supercooling) explains the difference of temperature between (cold) crystallization and melting observed for  $\text{PYR}_{14}\text{DCA}$ . It is thus the first report concerning the crystallization and melting of  $\text{PYR}_{14}\text{DCA}$ .  $\text{PYR}_{14}\text{TFSI}$  phase behavior has been extensively investigated and its melting point is  $-3^\circ\text{C}$ [37]. On the contrary,  $\text{PYR}_{14}\text{TFSAM}$  does not exhibit any crystallization or melting, which extends its liquid range down to its  $T_g$ , as for  $\text{PYR}_{14}\text{FTFSI}$ [31]. In both cases, enhanced asymmetry results in amorphous ILs on a wide temperature range.

### 3.2 Density, Viscosity and Conductivity

The variation of the densities for  $\text{PYR}_{14}\text{TFSAM}$  and  $\text{PYR}_{14}\text{DCA}$  with temperature have been measured and are compared with those of  $\text{PYR}_{14}\text{TFSI}$  in figure 2b. As can be seen, the density of  $\text{PYR}_{14}\text{TFSAM}$  stands, logically, in between those of the two other ILs. The variation with temperature is linear and can be fitted with equation (1) and the parameters reported in table 2.

$$\rho = \rho_0 + aT \quad (1)$$

The viscosities of  $\text{PYR}_{14}\text{DCA}$  and  $\text{PYR}_{14}\text{TFSAM}$  are compared with that of  $\text{PYR}_{14}\text{TFSI}$ [28],  $\text{PYR}_{14}\text{FSI}$ [38] and  $\text{PYR}_{14}\text{FTFSI}$ [31] in figure 2d.  $\text{PYR}_{14}\text{TFSI}$  exhibits, by far, the highest viscosity, while  $\text{PYR}_{14}\text{DCA}$  has the lowest on the whole temperature range.  $\text{PYR}_{14}\text{TFSAM}$ , however, performs not only better than  $\text{PYR}_{14}\text{FTFSI}$ , but similarly to  $\text{PYR}_{14}\text{FSI}$ , especially above  $30^\circ\text{C}$ , as its viscosity becomes lower. The data have been fitted with the Vogel-Tammann-Fulcher (VTF) equation (2), with  $X = \eta$  (dynamic viscosity),  $X_\infty = \eta_\infty$  and the corresponding parameters are reported in table 2.

$$X = X_\infty e^{\left(\frac{B}{T-T_0}\right)} \quad (2)$$

The conductivities of the pure ILs are reported on figure 3a. and compared to those incorporating other anions (FSI, FTFSI, TFSI, and the 4,5 dicyano-2-(trifluoromethyl)imidazole anion (TDI)). TDI is an

aromatic anion, which incorporates two  $-\text{CN}$  substituents as well as one  $-\text{CF}_3$  group[39,40] and it has been reported recently as high temperature alternative to  $\text{PYR}_{14}\text{TFSI}$ , despite its high melting point[41].

$\text{PYR}_{14}\text{TFSAM}$  has a conductivity halfway between  $\text{PYR}_{14}\text{DCA}$  and  $\text{PYR}_{14}\text{TFSI}$ , whereas  $\text{PYR}_{14}\text{FTFSI}$  is closer to  $\text{PYR}_{14}\text{FSI}$  than  $\text{PYR}_{14}\text{TFSI}$ . However, given the much higher conductivity of  $\text{PYR}_{14}\text{DCA}$  ( $10.3 \text{ mS cm}^{-1}$  at  $20^\circ\text{C}$ ) as compared with  $\text{PYR}_{14}\text{FSI}$ ,  $\text{PYR}_{14}\text{TFSAM}$  still reaches  $3.8 \text{ mS cm}^{-1}$  at  $20^\circ\text{C}$ , which is higher than  $\text{PYR}_{14}\text{FTFSI}$ . In fact, it can be seen that the conductivities of  $\text{PYR}_{14}\text{FSI}$  are higher than those of  $\text{PYR}_{14}\text{TFSAM}$  in the temperature range investigated, but that the curves seem to cross at higher temperature and the conductivities at  $60^\circ\text{C}$  are close, in accordance with the lower viscosity of  $\text{PYR}_{14}\text{TFSAM}$  at higher temperatures. The conductivities of  $\text{PYR}_{14}\text{DCA}$  and  $\text{PYR}_{14}\text{TFSAM}$  have been fitted by equation (2) with  $X = \sigma$ ,  $X_\infty = \sigma_\infty$ ,  $B = B'$  and  $T_0 = T_0'$  and the corresponding parameters are reported in table 2. The 'ideal' glassy transition temperature determined for viscosity and conductivity,  $T_0$  and  $T_0'$ , are very close to each other (and from one IL to the other) and roughly  $20^\circ\text{C}$  below the experimental  $T_g$ s. For  $\text{PYR}_{14}\text{TFSI}$ , the reported  $T_0'$  is  $182 \text{ K}$  [30], which agrees with its higher viscosity and higher  $T_g$ .

If we compare the curve of  $\text{PYR}_{14}\text{TDI}$ , the conductivities are much lower and there is an obvious gap in conductivity measurements as the IL crystallizes both during cooling ramp and heating ramp (on a quenched sample). However, above its melting point (at  $48^\circ\text{C}$ ),  $\text{PYR}_{14}\text{TDI}$  provides higher conductivities than  $\text{PYR}_{14}\text{TFSI}$ . However, in this case, the slope of the conductivity curve is even more marked than for  $\text{PYR}_{14}\text{TFSAM}$ , which results in lower conductivity at low temperatures, probably linked to the viscosity increase. In this case, not only the  $-\text{CN}$  groups, but also the rigid and planar structure might affect the low temperature viscosity and conductivity.

### FIGURE 3

For comparison, the conductivities of LiDCA and LiTFSAM in conventional 1M EC/DMC 1:1, wt mixtures have been measured and are shown in figure 3b. As can be seen, the order of conductivity is inverted, with a strong advantage for LiTFSAM with  $3.7 \text{ mS cm}^{-1}$  at  $20^\circ\text{C}$ , whereas LiDCA only leads to  $1.0 \text{ mS cm}^{-1}$ . In this case where the viscosity induced by the anion is not too severe,  $\text{DCA}^-$  does not present any conductivity advantage, which can be linked, *a priori*, to its lower dissociation whereas the small size of the anion bring significant advantage in the IL form..

On the other hand, the conductivity reached by LiTFSAM is higher, which can be attributed to the enhanced charge delocalization brought by the  $\text{SO}_2\text{-CF}_3$  group (also responsible for the increased anodic stability) and the resulting increase of ionic dissociation. The conductivity of LiTFSAM is, however, lower than many other Li salts. In fact, LiTDI, at  $20^\circ\text{C}$ , has a conductivity of  $6.7 \text{ mS cm}^{-1}$ , LiTFSI of  $9.0 \text{ mS cm}^{-1}$  [40] in similar conditions and LiFSI, at 0.85 M and  $25^\circ\text{C}$  of  $12 \text{ mS cm}^{-1}$ [13]. It shows that, in ILs, the size of the anion and the viscosity induced has a stronger effect on conductivity than lowering the coordination capability of the anion, which limits the possibility of improving conductivity by use of large anions. The comparison with the TDI<sup>-</sup> anion shows that, by use of aromatic charge delocalization, assisted by two  $-\text{CN}$  groups and one  $-\text{CF}_3$  electron withdrawing groups it is possible to reach a higher dissociation of the Li salt in EC/DMC, but that a high molecular weight, symmetry and rigidity are not favorable for a use as IL at moderate temperature, given the high viscosity and melting point.

The Walden plots of  $\text{PYR}_{14}\text{DCA}$ ,  $\text{PYR}_{14}\text{TFSI}$  and  $\text{PYR}_{14}\text{TFSAM}$  are shown in figure 3d., to get a better idea of the relation between conductivity and viscosity[42,43]. It is often considered that the ILs that fall well below the ‘*ideal KCl line*’ are more associated than those falling closer (thus a lower conductivity at similar viscosity) and those falling above this line are sometimes qualified as ‘*superionic liquids*’ [44], the position of the curve defining the ‘*ionicity*’ of an electrolyte. It is clear that  $\text{PYR}_{14}\text{DCA}$  falls closer to the line than  $\text{PYR}_{14}\text{TFSI}$ .  $\text{PYR}_{14}\text{TFSAM}$  seems to have an ‘*ionicity*’ comparable to that of  $\text{PYR}_{14}\text{TFSI}$  at low fluidity, which, however, gets higher as the fluidity increases (at higher temperatures). In fact, its evolution is parallel to the ‘*ideal KCl line*’, while the two other salts get further

within increasing fluidity. It indicates that its ‘*ionicity*’ is rather constant and that its viscosity evolution mostly explains its conductivity behavior.

It is worth noticing that the trend for ‘*ionicity*’ does follow the opposite to that of dissociation in conventional EC/DMC solvent. It seems that, rather than the decrease of the  $\text{PYR}_{14}^+$ -anion interaction going from  $\text{DCA}^-$  to TFSI $^-$ , the size of the anion play a paramount role in ‘*ionicity*’, besides the effect on viscosity. This was already noticed for some  $\text{BF}_4^-$ -based ionic liquids, which show a ‘*superionic*’ character[44][45], whereas  $\text{LiBF}_4$  is not known for its good dissociation in conventional EC/DMC mixtures (as compared with  $\text{LiPF}_6$  or  $\text{LiTFSI}$ ).

When the Li salt is introduced into the ILs, the conductivity drops, as the interaction between the anion and  $\text{Li}^+$  is stronger than that between  $\text{PYR}_{14}^+$  and the anion. This is observed on figure 3c. for both  $\text{PYR}_{14}\text{DCA}$  and  $\text{PYR}_{14}\text{TFSAM}$ . However, the conductivity drop, in the case of  $\text{PYR}_{14}\text{TFSAM}$  is more marked in the presence of  $\text{LiTFSAM}$ . In particular, the  $\text{PYR}_{14}\text{DCA}$  electrolyte show 37% and 50% conductivity drops at 0.4M and 0.6M respectively, while for  $\text{PYR}_{14}\text{TFSAM}$ , the drops are 51% and 66% at 20°C. These conductivity drops decrease with increasing temperature and the conductivities of the 0.4M electrolytes, at 60°C are  $7.4 \text{ mS cm}^{-1}$  for  $\text{PYR}_{14}\text{TFSAM}$  and  $19.9 \text{ mS cm}^{-1}$  for  $\text{PYR}_{14}\text{DCA}$ .

### 3.3 Electrochemical stability windows

#### FIGURE 4

The electrochemical stability window (ESW) of  $\text{PYR}_{14}\text{TFSAM}$  and  $\text{PYR}_{14}\text{DCA}$  electrolytes are shown figure 4. As can be seen, the anodic stability of  $\text{PYR}_{14}\text{DCA}$  is similar to that published for ethyl-methyl imidazolium  $\text{DCA}^-$  [21], with a decomposition at ca. 3.5 V vs  $\text{Li}^+/\text{Li}$ , which is, *a priori*, too low for most Li-ion battery application. The current do not increase significantly and decreases at high potential, which probably indicates (partial) passivation of the electrode. The stability in reduction is also quite low with reduction reaction starting at ca. 1.5V.

$\text{PYR}_{14}\text{TFSAM}$ , on the contrary, shows excellent stability in oxidation, with negligible current up to 4.5V vs  $\text{Li}^+/\text{Li}$ , which shows that the replacement of one -CN group by a  $-\text{SO}_2-\text{CF}_3$  allows significantly lowering the HOMO of the anion and increase both the anodic stability and the dissociation in EC/DMC.

The cathodic stability of  $\text{PYR}_{14}\text{TFSAM}$  is also rather low, with a decomposition starting even before that of  $\text{PYR}_{14}\text{DCA}$ , at *ca.* 1.9 V vs  $\text{Li}^+/\text{Li}$ .

The addition of the Li salt at 0.4M has a positive effect for both ILs concerning the cathodic stability, as the extensive reduction currents convert into small peaks, which indicates that surface reactions take place and that the passivation of the electrode, limits further electrolyte reactivity. This is known that the Li salt plays a paramount role in SEI formation in ILs[46] and allow, for instance using some ILs/Li salt mixtures for Li plating [47,48] with ILs which, alone, would decompose prior to Li deposition. In the case of  $\text{PYR}_{14}\text{TFSAM}$ , the current is then rather low until Li plating occurs, although a small reduction wave can be seen at *ca.* 0.4V. In the case of  $\text{PYR}_{14}\text{DCA}$ , further decomposition start slightly below 1.0 V vs  $\text{Li}^+/\text{Li}$ . There is no marked effect on the stability in oxidation linked to the Li salt and oxidation currents are overall increased, including, for the  $\text{PYR}_{14}\text{DCA}$  electrolyte, a stronger background current from OCP.

The use of vinylene carbonate (VC), a well-known SEI forming additive for conventional [49] and IL-based [50] electrolytes has a further effect on decreasing reduction currents, for both ILs. In the case of  $\text{PYR}_{14}\text{TFSAM}$ , after a small peak starting at *ca.* 1.6 V vs  $\text{Li}^+/\text{Li}$ , the background currents, prior to Li deposition are lower than  $2 \mu\text{A cm}^{-2}$ . They are higher for the VC-containing  $\text{PYR}_{14}\text{DCA}$  electrolyte and, in addition, a further decomposition step occurs at *ca.* 100 mV vs  $\text{Li}^+/\text{Li}$ .

Thus, it seems that the 0.4 M  $\text{LiTFSAM}$   $\text{PYR}_{14}\text{TFSAM}$  electrolyte (with or without VC) is a good candidate for Li-ion or Li metal application combining at the same time a 4.5V anodic stability and good passivation properties in reduction. However, as in Li-ion electrodes, surface groups, defects, current collectors and higher surface areas can influence the practical ESW, further testing was conducted with lithium metal, graphite and NCM cathodes.

#### Lithium plating /stripping

### FIGURE 5

The plating/stripping behavior of Li metal has been tested in  $\text{PYR}_{14}\text{TFSAM}$  with and without VC (the curve obtained without  $\text{LiTFSAM}$  is shown for comparison). The voltammograms show plating and

stripping in both cases, with the reaching of the same steady-state (diffusion limited), current at *ca.* 150  $\mu\text{A cm}^{-2}$  at the end of the plating step (which is above, for instance, the limiting current reported for LiTDI/PYR<sub>14</sub>TDI at 60°C [[41]). On the reverse scan, in both cases, Li stripping occurs. However, it is clear that, with the addition of VC, the Li stripping peaks is larger. By doing the ratio of the capacities, coulombic efficiencies for Li plating/stripping of 37.8% without VC and of 55.7% with VC have been calculated. The lithium plating/stripping conditions are not ideal, considering the very low reversing potential of -500 mV vs Li<sup>+</sup>/Li and the dendritic deposition of lithium occurring *a priori* when steady state-current is reached (especially as Ni is not, in general, ideal to realize homogeneous Li plating[51]). Nevertheless, it shows that the electrolytes are able to deposit Li metal even if the ptimization of the Li metal performance is beyond the scope of the present study.

The insertion of Li<sup>+</sup> into graphite has been probed by cyclic voltammetry at room temperature. Figure 5c. shows the four first voltammograms at 20°C. As can be seen, in the first cycle, a first reduction peak starts slightly below 2.0V and another is visible at *ca.* 0.8V and overlaps with Li<sup>+</sup> insertion into graphite. On the reversed scan, significant amount of Li<sup>+</sup> is de-inserted from the graphite electrode and it is possible to see several peaks corresponding to the different stages of Li<sup>+</sup> insertion into graphite. The current density increase with cycling upon lithiation and the delithiation peaks also become more defined. This could be due either to slow wetting of the electrode or to the establishment of a more favorable SEI on the surface of graphite after the first cycle. The cycling of graphite seems possible which confirms that a SEI allowing Li<sup>+</sup> transport and preventing graphite exfoliation is formed. Galvanostatic cycling of graphite was also performed at 40°C and in this case, the different insertion stage of graphite are more marked and the curves of two consecutive cycles overlap, as illustrated in the insert of figure 5c.

#### Li<sup>+</sup> insertion into LiNi<sub>0.5</sub>Co<sub>0.2</sub>Mn<sub>0.3</sub>O<sub>2</sub> (NCM523)

The 0.4M IL-based electrolytes have been used to cycle NCM cathodes at 40°C and the results are shown in figures 5b. and 5d. Surprisingly, PYR<sub>14</sub>DCA allows cycling of NCM with a rather good efficiency in the first cycle (87.4%), which contrasts with its low anodic stability. It is very likely that a passivation layer forms and protect the cathode. In fact, the oxidation currents on Pt (see figure 4) are

rather low and in the form of peaks, which already suggested a passivation of the Pt electrode. On the contrary, no feature is observed on the voltage profile that would correspond to extensive decomposition of the electrolyte. While this relatively good cycling performance deserves further investigations, the capacity decay with cycling is still rather marked, with a 14% decay in 30 cycles. Also, the efficiency raises after the first cycle but it does not reach more than 97% before starting decaying after 15 cycles.

On the other hand, the  $\text{PYR}_{14}\text{TFSAM}$  electrolyte exhibits a higher first cycle efficiency (92.6%) and the efficiencies then raise to 98.4% after 15 cycle before slightly decaying. The capacity retention is much improved, with a 90.5% capacity retention in the first 30 cycles. Several phenomena can influence the cycling stability of NCM half-cells such as the loss of active NCM, increase of electrolyte (and/or SEIs) resistance as well as slower  $\text{Li}^+$  diffusion in the SEIs. The voltage profiles, shown in inserts in figures 5b and d, overlap up to ca.  $90 \text{ mAh g}^{-1}$  during charge in both cases, as the equivalent series resistance (ESR) stays constant over cycling (i.e. no marked increase of electrolyte and SEI resistance). Also, a loss of active NCM would result in slope differences from the beginning of the charge. Thus, it is likely that the slope differences, above  $90 \text{ mAh g}^{-1}$ , result from an increase of  $\text{Li}^+$  mass transport limitation in some areas of the cells, either at the Li metal electrode or at the cathode. During discharge, differences between voltage plateaus can be explained by the lower state of charge reached at the end of the charge, in both cases. However, at the end of the plateau, the voltage curves stay parallel in the case of  $\text{PYR}_{14}\text{TFSAM}$ , which shows that the NMC electrode is fully lithiated at this point. On the other hand, for  $\text{PYR}_{14}\text{DCA}$ , the slope becomes less steep with cycling, which indicate  $\text{Li}^+$  mass transport limitation during NCM lithiation as well. It is thus likely, that in both cases the Li metal interface evolves toward slower  $\text{Li}^+$  transport (as seen in charge, corresponding to Li metal plating and NCM delithiation), but during discharge, only the  $\text{PYR}_{14}\text{DCA}$  cell evolve toward slower mass transport, which is a clue of passivation layer formation at the cathode with this electrolyte.

such as Mn dissolution, especially at  $40^\circ\text{C}$ ). Nevertheless, these results, although preliminary, do not show extensive electrolyte decomposition in neither electrolytes. It is, moreover, clear that the higher oxidative stability of  $\text{PYR}_{14}\text{TFSAM}$  allows better cycling performance, as compared with  $\text{PYR}_{14}\text{DCA}$ , but the excellent results obtained with  $\text{PYR}_{14}\text{DCA}$  contrast with its low anodic stability on Pt. This

promising result should be confirmed in full Li-ion cells as the Li metal counter electrode, especially at moderate rate, might influence the performance due to the production of reduction products in the electrolyte, which can diffuse to the cathode and be oxidized [52].

### 3.4 Al current collector corrosion

While TFSI-based ILs have been shown to prevent, to certain extent, Al current collector corrosion[53], it is still an issue with LiTFSI in common alkyl carbonate mixture or in FSI containing ILs [54]. Thus, LiTFSAM has been tested in EC/DMC for Al corrosion by chronoamperometry. Figure 6 shows the comparison between LiTFSI and LiTFSAM in EC/DMC using a piece of Al current collector at 4.2V vs (Li<sup>+</sup>/Li). As can be seen, the current increase rather quickly in the case of LiTFSI, whereas it decreases in the case of LiTFSAM (it increases after few hours, probably due to the Li metal counter electrode used in the experiment). These result is of high practical interest as Li salts which do not induce Al corrosion in EC/DMC, corrode even less in IL-based electrolyte including the same anion.

## FIGURE 6

### Conclusion

We presented an evaluation of PYR<sub>14</sub>TFSAM in view of use in Li-ion batteries with a focus on the comparison with its parent ILs (PYR<sub>14</sub>DCA and PYR<sub>14</sub>TFSI), as well as other reported PYR<sub>14</sub>-based ILs. It was shown that TFSAM possesses a higher thermal and anodic stability as compared with PYR<sub>14</sub>DCA PYR<sub>14</sub>FSI and PYR<sub>14</sub>FTFSI and that its conductivity is higher than that of PYR<sub>14</sub>TFSI and PYR<sub>14</sub>FTFSI at room temperature (and close to that of PYR<sub>14</sub>FSI at 60°C). PYR<sub>14</sub>TFSAM does not crystallize, which extends its possible use to low temperature applications. The presence of LiTFSAM in the electrolyte considerably extend its ESW in reduction and allows deposition of Li metal. The addition of VC as SEI forming additive improves further the SEI formation, allowing an improvement of the lithium plating/stripping efficiency as well as Li<sup>+</sup> (de)-insertion into graphite at room temperature or at 40°C. Finally, cycling of NCM Li-ion cathode was demonstrated at 40°C in PYR<sub>14</sub>TFSAM-based electrolyte but also, surprisingly (although with lower performances) in PYR<sub>14</sub>DCA-based electrolyte.

### Acknowledgements:

The research presented has been partly funded by the ‘SPICY’ project funded by the European Union’s Horizon 2020 research and innovation program under grant agreement N° 653373. The research presented here will be the base of further investigations which will be done within the GrEEn project, funded by the Nordrhein-Westfalen region of Germany. Moreover, E.P. would like to thank Dr. Sébastien Fantini and the company Solvionic S.A. for providing the PYR<sub>14</sub>TDI and LiTDI materials free of charge. Dr. G. Appetecchi (ENEA, Italy) is also gratefully acknowledged for providing the data on PYR<sub>14</sub>TFSI from ref [28].

## References

- [1] P. Isken, C. Dippel, R. Schmitz, R.W. Schmitz, M. Kunze, S. Passerini, M. Winter, A. Lex-Balducci, High flash point electrolyte for use in lithium-ion batteries, *Electrochim. Acta.* 56 (2011) 7530–7535. doi:10.1016/j.electacta.2011.06.095.
- [2] C.G. Barlow, Reaction of water with hexafluorophosphates and with Li bis(perfluoroethylsulfonyl)imide salt, *Electrochem. Solid-State Lett.* 2 (1999) 362–364. doi:10.1149/1.1390838.
- [3] H. Yang, G. V. Zhuang, P.N. Ross, Thermal stability of LiPF<sub>6</sub> salt and Li-ion battery electrolytes containing LiPF<sub>6</sub>, *J. Power Sources.* 161 (2006) 573–579. doi:10.1016/j.jpowsour.2006.03.058.
- [4] C.L. Campion, W. Li, B.L. Lucht, Thermal Decomposition of LiPF<sub>6</sub>-Based Electrolytes for Lithium-Ion Batteries, *J. Electrochem. Soc.* 152 (2005) A2327. doi:10.1149/1.2083267.
- [5] K. Xu, S. Zhang, J.L. Allen, T.R. Jow, Evaluation of Fluorinated Alkyl Phosphates as Flame Retardants in Electrolytes for Li-Ion Batteries: II. Performance in Cell, *J. Electrochem. Soc.* 150 (2003) A170. doi:10.1149/1.1533041.
- [6] X. Wang, E. Yasukawa, S. Kasuya, Nonflammable Trimethyl Phosphate Solvent-Containing Electrolytes for Lithium-Ion Batteries: II. The Use of an Amorphous Carbon Anode, *J. Electrochem. Soc.* 148 (2001) A1066. doi:10.1149/1.1397774.
- [7] C.A. Xu, K. Angell, High Anodic Stability of a New Electrolyte Solvent: Unsymmetric Noncyclic Aliphatic Sulfone, *J. Electrochem. Soc.* 145 (1998) L70. doi:10.1149/1.1838419.

- [8] Y. Abu-Lebdeh, I. Davidson, High-Voltage Electrolytes Based on Adiponitrile for Li-Ion Batteries, *J. Electrochem. Soc.* 156 (2009) A60. doi:10.1149/1.3023084.
- [9] M. Dahbi, F. Ghamouss, F. Tran-Van, D. Lemordant, M. Anouti, Comparative study of EC/DMC LiTFSI and LiPF<sub>6</sub> electrolytes for electrochemical storage, *J. Power Sources.* 196 (2011) 9743–9750. doi:10.1016/j.jpowsour.2011.07.071.
- [10] H.B. Han, S.S. Zhou, D.J. Zhang, S.W. Feng, L.F. Li, K. Liu, W.F. Feng, J. Nie, H. Li, X.J. Huang, M. Armand, Z. Bin Zhou, Lithium bis(fluorosulfonyl)imide (LiFSI) as conducting salt for nonaqueous liquid electrolytes for lithium-ion batteries: Physicochemical and electrochemical properties, *J. Power Sources.* 196 (2011) 3623–3632. doi:10.1016/j.jpowsour.2010.12.040.
- [11] E. Peled, The Electrochemical Behavior of Alkali and Alkaline Earth Metals in Nonaqueous Battery Systems—The Solid Electrolyte Interphase Model, *J. Electrochem. Soc.* 126 (1979) 2047. doi:10.1149/1.2128859.
- [12] J.R. Fong, R. von Sacken U. Dahn, Studies of Lithium Intercalation into Carbons Using Nonaqueous Electrochemical Cells, *J. Electrochem. Soc.* 137 (1990) 2009–2013.
- [13] A. Abouimrane, J. Ding, I.J. Davidson, Liquid electrolyte based on lithium bis-fluorosulfonyl imide salt: Aluminum corrosion studies and lithium ion battery investigations, *J. Power Sources.* 189 (2009) 693–696. doi:10.1016/j.jpowsour.2008.08.077.
- [14] P.C. Howlett, D.R. MacFarlane, A.F. Hollenkamp, High Lithium Metal Cycling Efficiency in a Room-Temperature Ionic Liquid, *Electrochem. Solid-State Lett.* 7 (2004) A97. doi:10.1149/1.1664051.
- [15] E. Paillard, Q. Zhou, W.A. Henderson, G.B. Appetecchi, M. Montanino, S. Passerini, Electrolytes with LiFSI FSI -Based 14 Electrochemical and Physicochemical Properties of PY Electrochemical and Physicochemical Properties of PY 14 FSI-Based Electrolytes with LiFSI, *J. Electrochem. Soc.* 156 (2009) 891–895. doi:10.1149/1.3208048.
- [16] J.H. Shin, W.A. Henderson, S. Passerini, Ionic liquids to the rescue? Overcoming the ionic conductivity limitations of polymer electrolytes, *Electrochem. Commun.* 5 (2003) 1016–1020. doi:10.1016/j.elecom.2003.09.017.

- [17] I. Osada, J. Von Zamory, E. Paillard, S. Passerini, Improved lithium-metal/vanadium pentoxide polymer battery incorporating crosslinked ternary polymer electrolyte with N-butyl-N-methylpyrrolidinium bis(perfluoromethanesulfonyl)imide, *J. Power Sources*. 271 (2014) 334–341. doi:10.1016/j.jpowsour.2014.08.019.
- [18] M. Ishikawa, T. Sugimoto, M. Kikuta, E. Ishiko, M. Kono, Pure ionic liquid electrolytes compatible with a graphitized carbon negative electrode in rechargeable lithium-ion batteries, *J. Power Sources*. 162 (2006) 658–662. doi:10.1016/j.jpowsour.2006.02.077.
- [19] M. Yamagata, K. Tanaka, Y. Tsuruda, Y. Sonem, S. Fukuda, S. Nakasuka, M. Kono, Ishikawa, *Electrochemistry*, (2015).
- [20] L. Grande, E. Paillard, G.T. Kim, S. Monaco, S. Passerini, Ionic liquid electrolytes for Li-air batteries: Lithium metal cycling, *Int. J. Mol. Sci.* 15 (2014) 8122–8137.
- [21] D.R. MacFarlane, S.A. Forsyth, J. Golding, G.B. Deacon, Ionic liquids based on imidazolium, ammonium and pyrrolidinium salts of the dicyanamide anion, *Green Chem.* 4 (2002) 444–448. doi:10.1039/b205641k.
- [22] H. Yoon, G.H. Lane, Y. Shekibi, P.C. Howlett, M. Forsyth, A.S. Best, D.R. MacFarlane, Lithium electrochemistry and cycling behaviour of ionic liquids using cyano based anions, *Energy Environ. Sci.* 6 (2013) 979–986. doi:10.1039/C3EE23753B.
- [23] S. Shen, S. Fang, L. Qu, D. Luo, L. Yang, S. Hirano, Low-viscosity ether-functionalized pyrazolium ionic liquids based on dicyanamide anions: properties and application as electrolytes for lithium metal batteries, *RSC Adv.* 5 (2015) 93888–93899. doi:10.1039/C5RA17539A.
- [24] C. Wolff, S. Jeong, E. Paillard, A. Balducci, S. Passerini, High power, solvent-free electrochemical double layer capacitors based on pyrrolidinium dicyanamide ionic liquids, *J. Power Sources*. 293 (2015) 65–70. doi:10.1016/j.jpowsour.2015.05.065.
- [25] E. Paillard, Q. Zhou, W.A. Henderson, G.B. Appetecchi, M. Montanino, S. Passerini, Electrochemical and Physicochemical Properties of PY<sub>14</sub>FSI-Based Electrolytes with LiFSI, *J. Electrochem. Soc.* 156 (2009) A891.
- [26] Q. Zhou, P.D. Boyle, L. Malpezzi, A. Mele, J.-H. Shin, S. Passerini, W.A. Henderson, Phase

- Behavior of Ionic Liquid–LiX Mixtures: Pyrrolidinium Cations and TFSI – Anions – Linking Structure to Transport Properties, *Chem. Mater.* 23 (2011) 4331–4337.  
doi:10.1021/cm201427k.
- [27] I. Rey, P. Johansson, J. Lindgren, J.C. Lasse, Spectroscopic and Theoretical Study of (CF<sub>3</sub>SO<sub>2</sub>)<sub>2</sub>N – (TFSI –) and (CF<sub>3</sub>SO<sub>2</sub>)<sub>2</sub>NH (HTFSI), *J. Phys. Chem. A.* 102 (1998) 3249–3258. doi:10.1021/jp980375v.
- [28] G.B. Appetecchi, M. Montanino, D. Zane, M. Carewska, F. Alessandrini, S. Passerini, Effect of the alkyl group on the synthesis and the electrochemical properties of N-alkyl-N-methyl-pyrrolidinium bis(trifluoromethanesulfonyl)imide ionic liquids, *Electrochim. Acta.* 54 (2009) 1325–1332. doi:10.1016/j.electacta.2008.09.011.
- [29] H. Matsumoto, N. Terasawa, T. Umecky, S. Tsuzuki, H. Sakaebe, K. Asaka, K. Tatsumi, Low Melting and Electrochemically Stable Ionic Liquids Based on Asymmetric Fluorosulfonyl(trifluoromethylsulfonyl)amide, *Chem. Lett.* 37 (2008) 1020–1021. doi:10.1246/cl.2008.1020.
- [30] G.B. Appetecchi, M. Montanino, M. Carewska, M. Moreno, F. Alessandrini, S. Passerini, Chemical-physical properties of bis(perfluoroalkylsulfonyl)imide-based ionic liquids, *Electrochim. Acta.* 56 (2011) 1300–1307. doi:10.1016/j.electacta.2010.10.023.
- [31] J. Reiter, S. Jeremias, E. Paillard, M. Winter, S. Passerini, Fluorosulfonyl-(trifluoromethanesulfonyl)imide ionic liquids with enhanced asymmetry, *Phys. Chem. Chem. Phys. Phys. Chem. Chem. Phys.* 15 (2013) 2565–2571. doi:10.1039/c2cp43066e.
- [32] M. Kunze, S. Jeong, E. Paillard, M. Winter, S. Passerini, Melting behavior of pyrrolidinium-based ionic liquids and their binary mixtures, *J. Phys. Chem. C.* 114 (2010) 12364–12369.
- [33] M. Montanino, M. Moreno, F. Alessandrini, G.B. Appetecchi, S. Passerini, Q. Zhou, W.A. Henderson, Physical and electrochemical properties of binary ionic liquid mixtures: (1-x) PYR14TFSI-(x) PYR14IM14, *Electrochim. Acta.* 60 (2012) 163–169. doi:10.1016/j.electacta.2011.11.030.
- [34] A.S. Shaplov, E.I. Lozinskaya, P.S. Vlasov, S.M. Morozova, D.Y. Antonov, P.-H. Aubert, M. Armand, Y.S. Vygodskii, New family of highly conductive and low viscosity ionic liquids with

- asymmetric 2,2,2-trifluoromethylsulfonyl-N-cyanoamide anion, *Electrochim. Acta.* (2015).  
doi:10.1016/j.electacta.2015.02.228.
- [35] A.P. Purdy, E. Houser, C.F. George, Lithium dicyanamide, its reactions with cyanuric chloride, and the crystal structures of  $\text{LiN}(\text{CN})_2(\text{MeCN})_2$  and  $\text{LiCN}(\text{C}_5\text{H}_5\text{N})_2$ , *Polyhedron.* 16 (1997) 3671–3679. doi:10.1016/S0277-5387(97)00097-1.
- [36] J.H. Shin, E.J. Cairns, N-Methyl-(n-butyl)pyrrolidinium bis(trifluoromethanesulfonyl)imide-LiTFSI-poly(ethylene glycol) dimethyl ether mixture as a Li/S cell electrolyte, *J. Power Sources.* 177 (2008) 537–545. doi:10.1016/j.jpowsour.2007.11.043.
- [37] W. a Henderson, S. Passerini, Phase Behavior of Ionic Liquid LiX Mixtures: Pyrrolidinium Cations and TFSI- Anions, *Chem. Mater.* 16 (2004) 2881–2885. doi:10.1021/cm049942j.
- [38] S. Passerini, E. Paillard, Q. Zhou, W.A. Henderson, G.B. Appetecchi, M. Montanino, Electrolytes with LiFSI FSI -Based 14 Electrochemical and Physicochemical Properties of PY Electrochemical and Physicochemical Properties of PY 14 FSI-Based Electrolytes with LiFSI, *J. Electrochem. Soc.* 156 (2009) 891–895. doi:10.1149/1.3208048.
- [39] L. Niedzicki, S. Grugeon, S. Laruelle, P. Judeinstein, M. Bukowska, J. Prejzner, P. Szczeciński, W. Wiczeorek, M. Armand, New covalent salts of the 4+ v class for Li batteries, *J. Power Sources.* 196 (2011) 8696–8700. doi:10.1016/j.jpowsour.2011.06.030.
- [40] L. Niedzicki, E. Karpierz, M. Zawadzki, M. Dranka, M. Kasprzyk, A. Zalewska, M. Marcinek, J. Zachara, U. Domańska, W. Wiczeorek, Lithium cation conducting TDI anion-based ionic liquids., *Phys. Chem. Chem. Phys.* 16 (2014) 11417–25. doi:10.1039/c3cp55354j.
- [41] A. Ochel, D. Di Lecce, C. Wolff, G.-T. Kim, D.V. Carvalho, S. Passerini, Physicochemical and electrochemical investigations of the ionic liquid N-butyl -N-methyl-pyrrolidinium 4,5-dicyano-2-(trifluoromethyl)imidazole, *Electrochim. Acta.* 232 (2017) 586–595.  
doi:10.1016/j.electacta.2017.02.141.
- [42] E.I. Cooper, C. a Angell, W. Lafayette, E . L Cooper , CA . Angell / Ambient temperature plastic crystal fast ion conductors, *Science* (80-. ). 19 (1986) 570–576.
- [43] C.A. Angell, (Invited) Ionic Liquids, Superionic Glasses, Quasi-Ionic Liquids, Quasi-Liquid Ionics, All with High Conductivities but Some with Little Fluidity. Where does the Paradigm

- End?, *ECS Trans.* 64 (2014) 9–20. doi:10.1149/06404.0009ecst.
- [44] C. Austen Angell, Y. Ansari, Z. Zhao, *Ionic Liquids: Past, present and future*, *Faraday Discuss.* 154 (2012) 9–27. doi:10.1039/C1FD00112D.
- [45] C. Schreiner, S. Zugmann, R. Hartl, H.J. Gores, Fractional walden rule for ionic liquids: Examples from recent measurements and a critique of the so-called ideal KCl line for the walden plot, *J. Chem. Eng. Data.* 55 (2010) 1784–1788. doi:10.1021/je900878j.
- [46] C. Liu, X. Ma, F. Xu, L. Zheng, H. Zhang, W. Feng, X. Huang, M. Armand, J. Nie, H. Chen, Z. Zhou, Ionic liquid electrolyte of lithium bis(fluorosulfonyl)imide/N-methyl-N-propylpiperidinium bis(fluorosulfonyl)imide for Li/natural graphite cells: Effect of concentration of lithium salt on the physicochemical and electrochemical properties, *Electrochim. Acta.* 149 (2014) 370–385. doi:10.1016/j.electacta.2014.10.048.
- [47] S. Ferrari, E. Quartarone, P. Mustarelli, A. Magistris, S. Protti, S. Lazzaroni, M. Fagnoni, A. Albini, A binary ionic liquid system composed of N-methoxyethyl-N-methylpyrrolidinium bis(trifluoromethanesulfonyl)-imide and lithium bis(trifluoromethanesulfonyl)imide: A new promising electrolyte for lithium batteries, *J. Power Sources.* 194 (2009) 45–50. doi:10.1016/j.jpowsour.2008.12.013.
- [48] J. Reiter, E. Paillard, L. Grande, M. Winter, S. Passerini, Physicochemical properties of N-methoxyethyl-N-methylpyrrolidinium ionic liquids with perfluorinated anions, *Electrochim. Acta.* 91 (2013) 101–107.
- [49] B. Simon, J.-P. Boeue, US 5,626,981, 1997.
- [50] M. Holzapfel, C. Jost, P. Novák, Stable cycling of graphite in an ionic liquid based electrolyte., *Chem. Commun. (Camb).* (2004) 2098–2099. doi:10.1039/b407526a.
- [51] L. Grande, J. Von Zamory, S.L. Koch, J. Kalhoff, E. Paillard, S. Passerini, Homogeneous Lithium Electrodeposition with Pyrrolidinium-Based Ionic Liquid Electrolytes, *ACS Appl. Mater. Interfaces.* 7 (2015) 5950–5958. doi:10.1021/acsami.5b00209.
- [52] J. Von Zamory, M. Bedu, S. Fantini, S. Passerini, E. Paillard, Polymeric ionic liquid nanoparticles as binder for composite Li-ion electrodes, *J. Power Sources.* 240 (2013) 745–752. doi:10.1016/j.jpowsour.2013.04.127.

- [53] R.S. Kühnel, M. Lübke, M. Winter, S. Passerini, A. Balducci, Suppression of aluminum current collector corrosion in ionic liquid containing electrolytes, *J. Power Sources*. 214 (2012) 178–184. doi:10.1016/j.jpowsour.2012.04.054.
- [54] E. Cho, J. Mun, O.B. Chae, O.M. Kwon, H.T. Kim, J.H. Ryu, Y.G. Kim, S.M. Oh, Corrosion/passivation of aluminum current collector in bis(fluorosulfonyl) imide-based ionic liquid for lithium-ion batteries, *Electrochem. Commun.* 22 (2012) 1–3. doi:10.1016/j.elecom.2012.05.018.

## Figure captions

**Figure 1.** Developed formulae of the bis(fluorosulfonyl) imide (FSI), bis(trifluoromethanesulfonyl) imide (TFSI), dicyanamide (DCA<sup>-</sup>), fluorosulfonyl-trifluoromethanesulfonyl imide (FTFSI) and trifluoromethanesulfonyl cyanoamide (TFSAM<sup>-</sup>) anions.

**Figure 2. (a)** TGA traces and weight loss derivative curves of PYR<sub>14</sub>DCA and PYR<sub>14</sub>TFSAM at 10°C min<sup>-1</sup> under N<sub>2</sub> and dry air. **(b)** Density of PYR<sub>14</sub>TFSI (taken from ref[30]), PYR<sub>14</sub>TFSAM and PYR<sub>14</sub>DCA. **(c)** DSC thermograms (heating ramp at 10°C min<sup>-1</sup> of PYR<sub>14</sub>TFSAM and PYR<sub>14</sub>DCA. **(d)** Viscosities of PYR<sub>14</sub>DCA and PYR<sub>14</sub>TFSAM, compared with those of PYR<sub>14</sub>FSI[38], PYR<sub>14</sub>TFSI[38] and PYR<sub>14</sub>FTFSI[31] **(insert)** VTF fit of the viscosities of PYR<sub>14</sub>DCA and PYR<sub>14</sub>TFSAM

**Figure 3. (a)** Conductivities of PYR<sub>14</sub>TDI, PYR<sub>14</sub>DCA, PYR<sub>14</sub>TFSAM compared with those of PYR<sub>14</sub>TFSI [28], PYR<sub>14</sub>FSI [38] and PYR<sub>14</sub>FTFSI [31]. **(insert)** VTF fit of the conductivities of PYR<sub>14</sub>DCA and PYR<sub>14</sub>TFSAM **(b)** Comparison of the conductivity in function of temperature for LiDCA and LiTFSAM in 1M EC/DMC 1:1, wt electrolyte solutions. **(c)** Conductivity in function of temperature for Li salts-containing electrolytes based on PYR<sub>14</sub>DCA and PYR<sub>14</sub>TFSAM **(d)** Walden plot of PYR<sub>14</sub>DCA, PYR<sub>14</sub>TFSAM and PYR<sub>14</sub>TFSI (from ref. [28])

**Figure 4.** Linear sweep voltametries in PYR<sub>14</sub>DCA, PYR<sub>14</sub>TFSAM and their 0.4M electrolytes with corresponding Li salt. Scan rate: 0.1 mV s<sup>-1</sup>. WE (anodic scan): Pt, WE (cathodic scan): Ni, CE: Li, RE: Li, 0.1 mV s<sup>-1</sup>

**Figure 5. (a)** Cyclic voltammograms of a Ni electrode in PYR<sub>14</sub>TFSAM, with and without addition of LiTFSAM and VC. Scan rate: 0.1 mV s<sup>-1</sup>. RE and CE: Li. **(b)** Cycling performance of NCM electrodes in 0.4 M LiDCA in PYR<sub>14</sub>DCA. **Inserts:** Corresponding voltage profiles for selected cycles. **(c)** Initial CV cycles of graphite electrode in 0.4 M LiTFSAM in PYR<sub>14</sub>TFSAM + 2 wt% VC. CE and RE: Li. Scan rate: 0.05 mV s<sup>-1</sup>. **(Insert):** Differential capacity plot of a similar cell cycled galvanostatically at C/10 and 40°C. 5<sup>th</sup> and 6<sup>th</sup> cycles shown. **(d)** Cycling performance of NCM electrodes in 0.4 M LiTFSAM in PYR<sub>14</sub>TFSAM.

**Figure 6.** Chronoamperometry at 4.2V of a Al electrode in 1M LiTFSI or 1M LiTFSAM in EC/DMC 1:1, wt electrolytes. RE: Li: CE: Li.

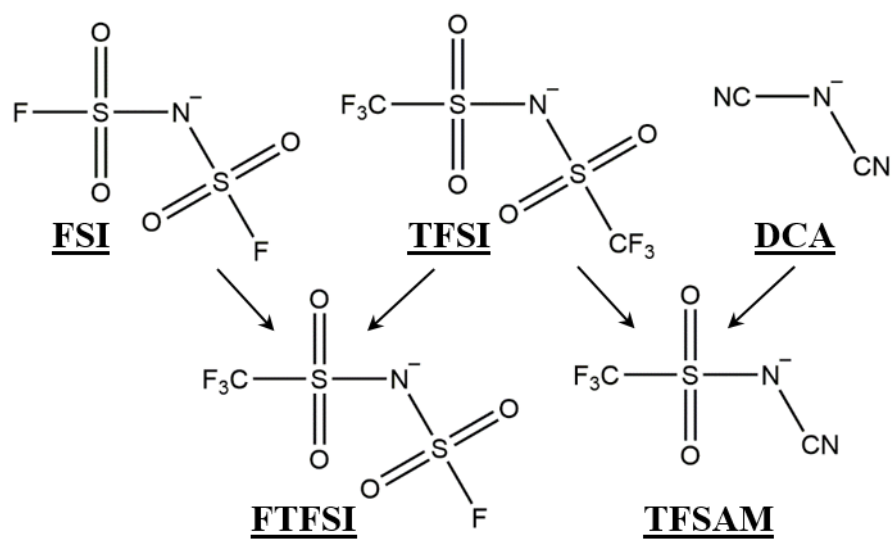


Figure 1.

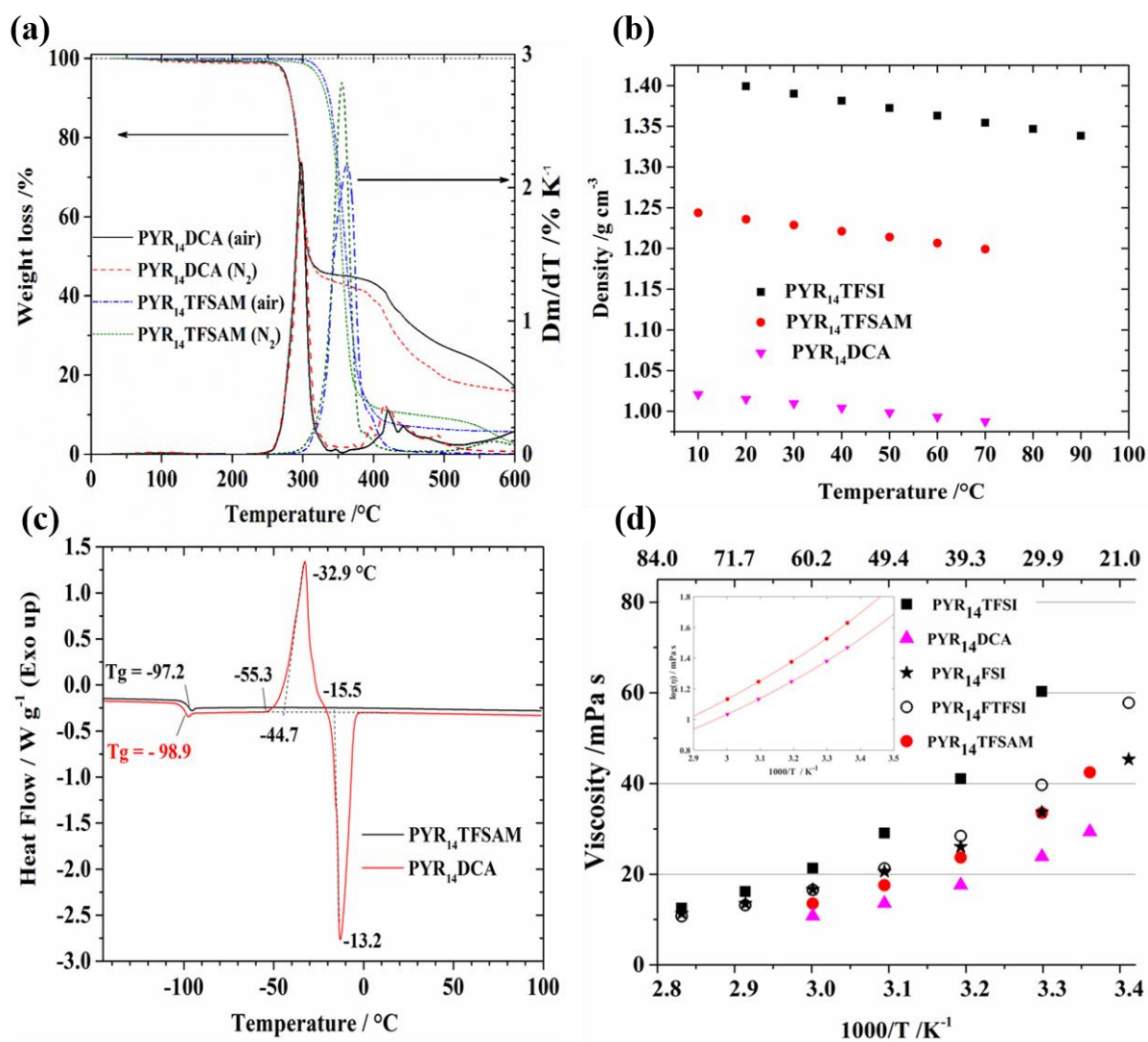


Figure 2.

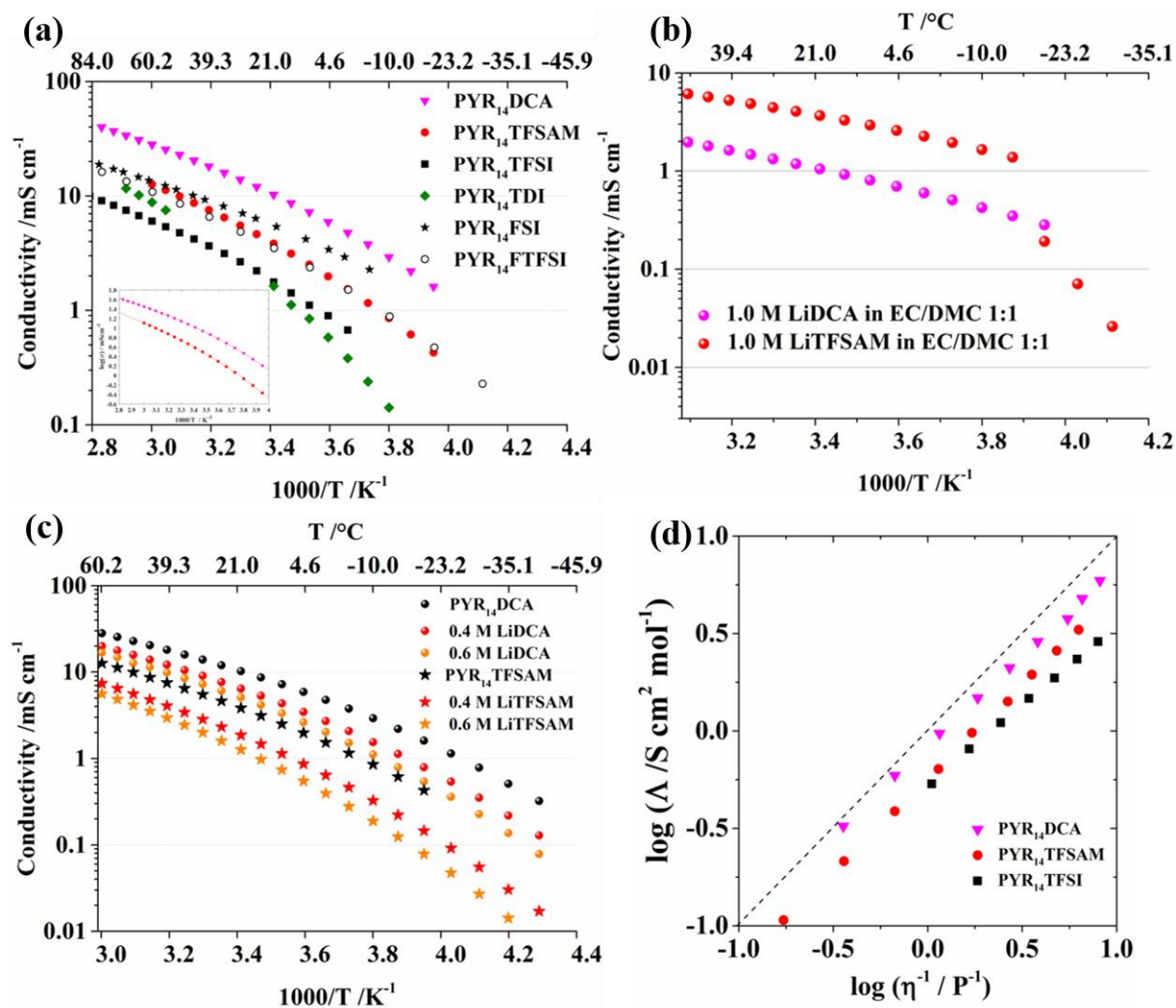


Figure 3.

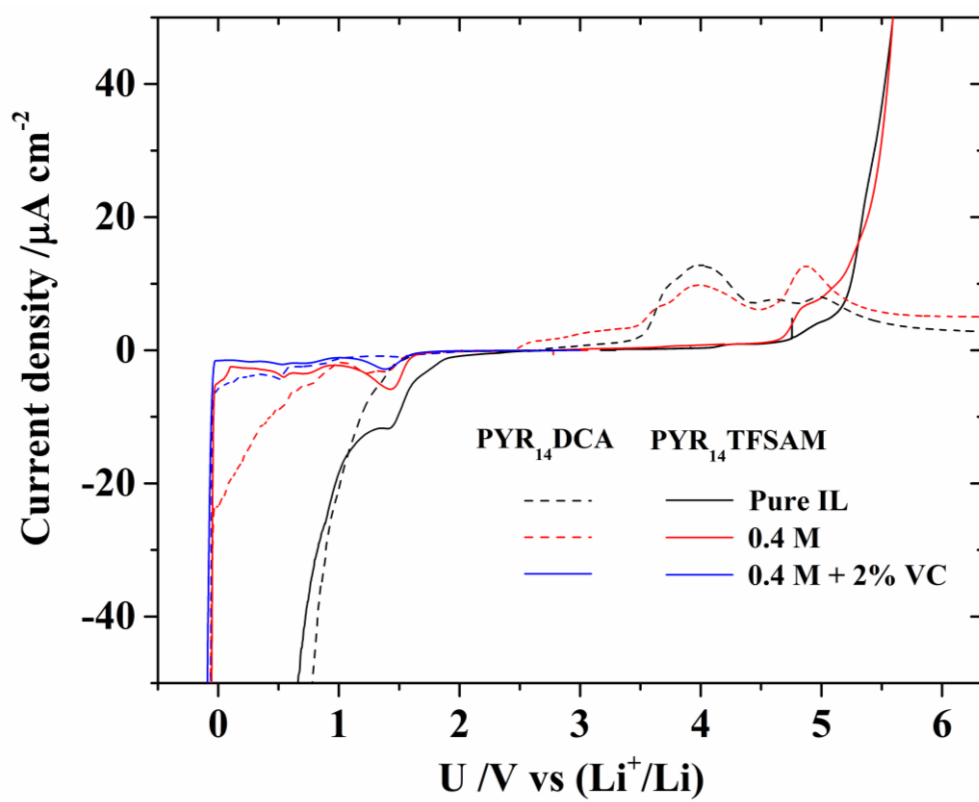


Figure 4.

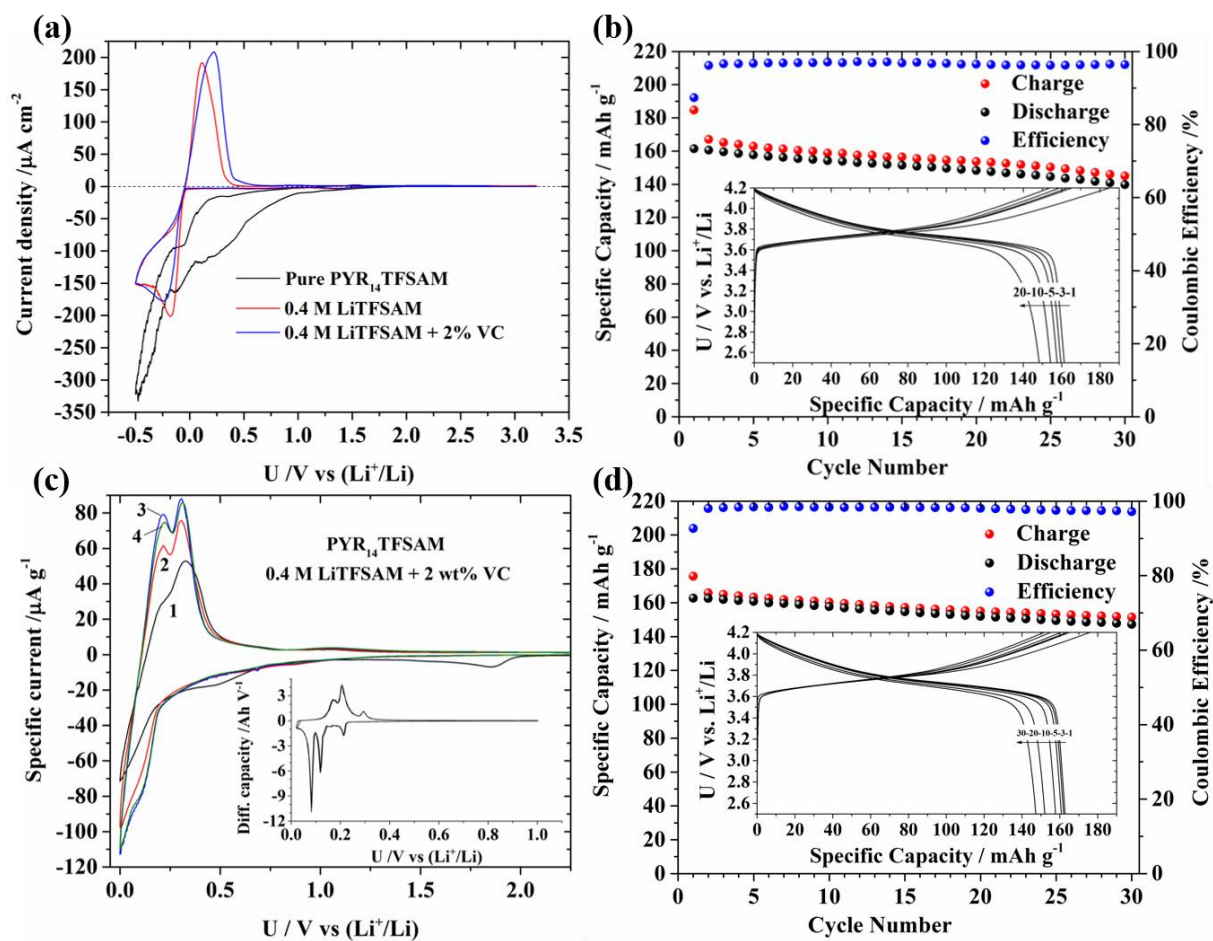


Figure 5.

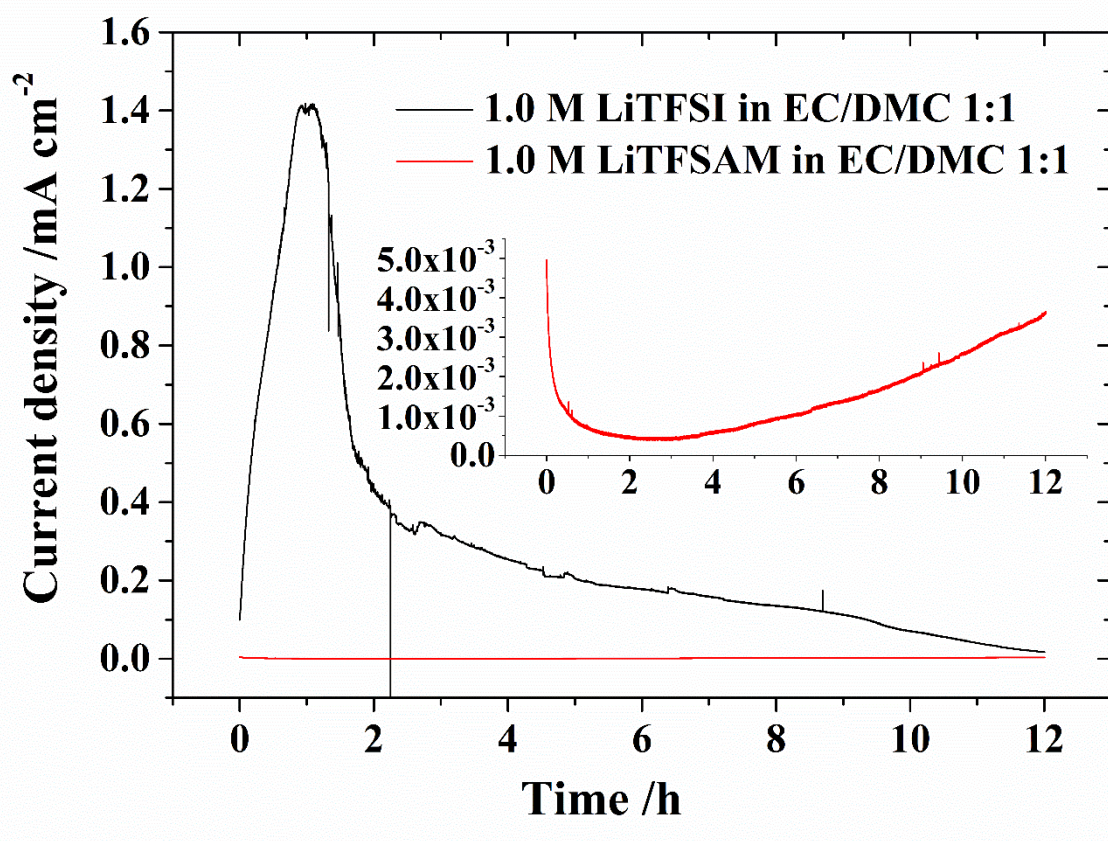


Figure 6.

**Table 1.** Thermal properties of PYR<sub>14</sub>DCA and PYR<sub>14</sub>TFSAM

<b>Ionic Liquid</b>	<b>T<sub>m</sub> / °C</b>	<b>ΔH<sub>m</sub> / J<sup>-1</sup></b>	<b>T<sub>c</sub> / °C</b>	<b>ΔH<sub>c</sub> / J g<sup>-1</sup></b>	<b>T<sub>g</sub> / °C</b>	<b>T<sub>dec.</sub> / °C (O<sub>2</sub> and N<sub>2</sub>)</b>
<b>PYR<sub>14</sub>DCA</b>	-15.5 <sup>1</sup>	110.0	-44.7	100.9	-98.9	238
<b>PYR<sub>14</sub>TFSAM</b>	-	-	-	-	-97.2	283

**Table 2.** Fitting parameters for density, viscosity and conductivity

<b>Ionic Liquid</b>	<b>ρ<sub>0</sub></b>	<b>a</b>	<b>η<sub>∞</sub></b>	<b>B</b>	<b>T<sub>0</sub></b>	<b>σ<sub>∞</sub></b>	<b>B'</b>	<b>T'<sub>0</sub></b>
	<b>/g cm<sup>-3</sup></b>	<b>/g cm<sup>-3</sup> °C<sup>-1</sup></b>	<b>/mPa s</b>	<b>/K</b>	<b>/K</b>	<b>/ mS cm<sup>-1</sup></b>	<b>/ K</b>	<b>/ K</b>
<b>PYR<sub>14</sub>TFSAM</b>	1.250	- 7.38 10 <sup>-4</sup>	0.19	784.6	155.2	779.0 ± 1.0	727.8	156.3
			± 0.02	± 45.0	± 3.7		± 9.3	± 0.8
<b>PYR<sub>14</sub>DCA</b>	1.026	- 5.52 10 <sup>-4</sup>	0.28	654.2 ±	158.5	916.9 ± 1.0	618.6 ±	155.5
			± 0.01	78.3	± 7.5		3.7	± 0.3

<sup>1</sup> T<sub>m</sub> is specified as the onset temperature of the endothermic melting peaks.



